NANO LETTERS

pubs.acs.org/NanoLett Letter

Anomalous Anisotropic Dopant Distribution in Hexagonal Yttrium Sublattice

Hongyu Bian, Caisheng Tang, He Zhao, Xian Qin,* and Xiaogang Liu*

Cite This: *Nano Lett.* 2023, 23, 979–984 Read Online

ACCESS | Metrics & More | Article Recommendations | Supporting Information

ABSTRACT: Trivalent lanthanides are commonly incorporated into sodium yttrium fluoride nanocrystals to enhance their optical properties. Lanthanides are expected to randomly replace trivalent yttrium cations due to their isovalent nature, and the dopant−dopant distance decreases with increasing dopant concentration. Combining spectroscopy with quantum mechanical calculations, we find that large lanthanides exhibit an anisotropic distribution in the hexagonal yttrium sublattice at low dopant concentrations. This counterintuitive substitution suggests the formation of one-dimensional dimers or chains with short dopant−dopant distances. Our study of the distance-sensitive cross-relaxation between Nd^{3+} dopants in β-$NaYF_4$ nanocrystals confirms that the concentration quenching threshold is lower than that of their cubic counterparts, consistent with the proposed chain-like model. Moreover, we demonstrate modulation of the anisotropic distribution by microstrain management via alkali metal codoping. Research into dopant distribution in inorganic crystals may enable the development of new materials and properties for future challenges.

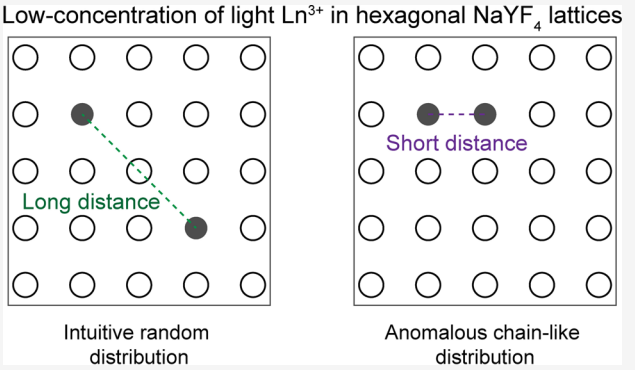

KEYWORDS: *downshifting, cross-relaxation, anisotropic substitution, lanthanides, concentration quenching*

Lanthanide doping into nanocrystals is widely used to enhance optical properties,[1−6] including photon upconversion and X-ray-activated ultralong afterglow.[7−16] Given its solution processability and low phonon energy (~360 cm^{-1}), hexagonal-phase sodium yttrium fluoride (β-$NaYF_4$) has been used as a host for lanthanide ions to prepare nanocrystals with diverse structural configurations.[17−21] It is possible to substitute host Y^{3+} cations with trivalent lanthanides (Ln^{3+}) to achieve 100% replacement due to their close match in ionic radius and charge valence. Lanthanide luminescence can be controlled in terms of wavelength and decay rate through doping concentration-dependent energy transfer.[22,23]

With increasing doping concentration, the distance between lanthanide dopants decreases.[24−29] Intuitively, random substitution of yttrium cations by trivalent lanthanides is expected at all doping concentrations, although there are two inequivalent Y_1 and Y_2 sites in the β-$NaYF_4$ host lattice (Figure S1). This is because both Y_1 and Y_2 cations have 9-coordinated fluoride anions with the tricapped trigonal prismatic geometry, as opposed to their cubic counterpart with one 8-coordinated Y site. Despite the rapid development of lanthanide-doped nanocrystals with versatile compositions and structural configurations, it remains a challenge to directly map lanthanide distribution in host sublattices, which imposes a stringent constraint on nanomanufacturing with atomic precision.

As a complement to experimental characterizations such as high-resolution transmission electron microscopy, first-principles calculations based on density functional theory (DFT) can accurately predict substitution sites in crystal lattices.[30−32] Additionally, spectroscopic characterization can be used to probe multipolar interactions between lanthanide ions, which gives information about their distances.[33] Here, by combining DFT calculations with spectroscopy characterization, we demonstrate that Y^{3+} ions are preferentially substituted in β-$NaYF_4$ lattices by light Ln^{3+} ions (La^{3+} to Sm^{3+}) at low doping concentrations, while heavy Ln^{3+} ions (Eu−Lu) show random substitution. In contrast to the traditional notion of uniform distribution, light Ln^{3+} dopants tend to form pairs or chain-like clusters with short Ln−Ln distances at low doping concentrations. Cross-relaxation-dictated emission lifetimes enable us to compare the distance between Nd^{3+} ions in β-$NaYF_4$ and its cubic counterpart.[34−36]

To study the substitution preference of lanthanide dopants, we calculated the electronic energies of β-$NaYF_4$ systems in

Received: November 12, 2022
Revised: January 10, 2023
Published: January 18, 2023

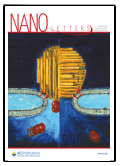

https://doi.org/10.1021/acs.nanolett.2c04454
Nano Lett. 2023, 23, 979−984

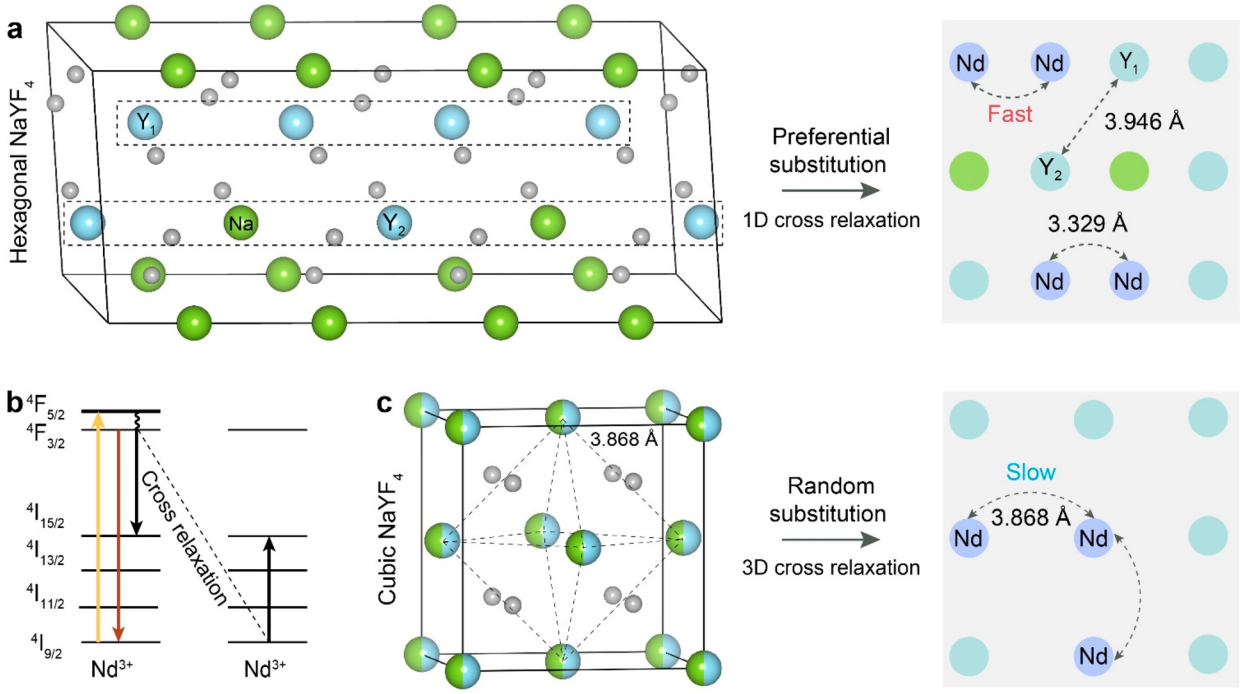

Figure 1. Cross-relaxation in lanthanide-doped $NaYF_4$ lattices. (a) Atomic structure of β-$NaYF_4$ and the corresponding illustration of the preferential substitution of Nd^{3+} for Y^{3+} host ions. Blue, green, purple, and gray spheres represent Y, Na, Nd, and F atoms, respectively. (b) Schematic of cross-relaxation between two Nd^{3+}. The yellow, red, and black straight arrows represent absorption, radiative decay, and nonradiative resonance energy transfer, respectively, while the curved black arrow denotes nonradiative decay. (c) Atomic structure of α-$NaYF_4$ and the corresponding illustration of the random substitution of Y^{3+} host ions by Nd^{3+} ions.

which Ln replaces Y_1 (Ln_{Y1}) or Y_2 (Ln_{Y2}) at doping concentrations of 4.2, 8.3, 17, and 33.3% (Figures 1a, S1, and S2). ΔE denotes the energy difference between β-$NaYF_4$:Ln_{Y2} and β-$NaYF_4$:Ln_{Y1} crystals. A positive value of ΔE indicates that the latter is more energetically stable than the former, and a large ΔE suggests a higher probability of substituting Ln for Y_1 atoms than Y_2. According to the calculated ΔE, we found that the first few elements of the lanthanide series prefer Y_1 over Y_2, while heavy elements feature random substitution, regardless of doping concentration. At a 4.2% doping concentration, this preferential substitution becomes more prominent for lanthanides with large ionic radii (La, Ce, Pr, and Nd). The underlying rationale is that lattice strain introduced by ionic radius misfits between Ln^{3+} and Y^{3+} can easily be released at the Y_1 site if they exceed 8% (Table S1). For example, we calculated the energies of β-$NaYF_4$:Nd crystals with nonrelaxed and relaxed atomic structures. The data show that the strain released at the Y_1 site lowers the energy of the β-$NaYF_4$:Nd system by 1.62 eV, which is 8-fold higher than that released at the Y_2 site. In this regard, Nd atoms are energetically more stable when replacing Y_1 atoms.

We next estimate the concentration of Nd_{Y1} and Nd_{Y2} substitutional defects using DFT-calculated formation energy E_f by

$$c = N_{site} \exp\left(-\frac{E_f}{kT}\right)$$

where N_{site} is the number of Y_1 or Y_2 sites in the fluoride lattice for which Nd^{3+} can substitute, k is the Boltzmann constant, and T is the temperature. The data show that the concentration of Nd_{Y1} is 6.4-fold higher than that of Nd_{Y2}.

Considering that Nd^{3+} ions show pronounced preferential substitution and feature distance-sensitive cross-relaxation, it is possible to capture the substitutional behavior of lanthanide ions in β-$NaYF_4$ lattices by measuring the luminescence lifetime of Nd^{3+} (Figure 1b). Specifically, Nd dopants tend to occupy Y_1 sites and form Nd−Nd pairs or chain-like clusters along the (0001) direction of the hexagonal lattice at low doping concentrations. We employed slab models to study the formation of Nd−Nd pairs during the growth of β-$NaYF_4$ crystals along the (0001) direction. On the basis of calculated electronic energies, two Nd atoms are more likely to replace two neighboring Y_1 atoms than one Y_1 and one Y_2 atom (Figure S3). Consequently, this substitutional configuration should lead to intense one-dimensional cross-relaxation and a low concentration quenching threshold because of the short distance between Nd^{3+} (3.329 Å). In contrast, the distance of an Nd−Nd pair (3.868 Å) in α-$NaYF_4$ is larger than that in the hexagonal lattice. This means that randomly doped α-$NaYF_4$ should exhibit slower three-dimensional cross-relaxation and a higher concentration quenching threshold (Figure 1c).

To validate this hypothesis, we synthesized a series of Nd-doped cubic and hexagonal $NaYF_4$ nanocrystals (α-$NaYF_4$:Nd and β-$NaYF_4$:Nd) with different doping concentrations of neodymium.[37] For the α-$NaYF_4$:Nd nanoparticles, transmission electron microscopy (TEM) images reveal uniform quasi-spherical morphology of the nanoparticles with an average size of ~6.8 nm (Figures 2a and S4). In the case of β-$NaYF_4$:Nd nanoparticles, TEM images show a size distribution between 4.7 and 5.5 nm (Figures 2b and S4). X-ray diffraction (XRD) characterizations confirm the pure phases of α- and β-$NaYF_4$:Nd nanoparticles (Figure 2c,d). A slight difference in diameter between cubic and hexagonal phase nanoparticles has little effect on the luminescence

https://doi.org/10.1021/acs.nanolett.2c04454
Nano Lett. 2023, 23, 979−984

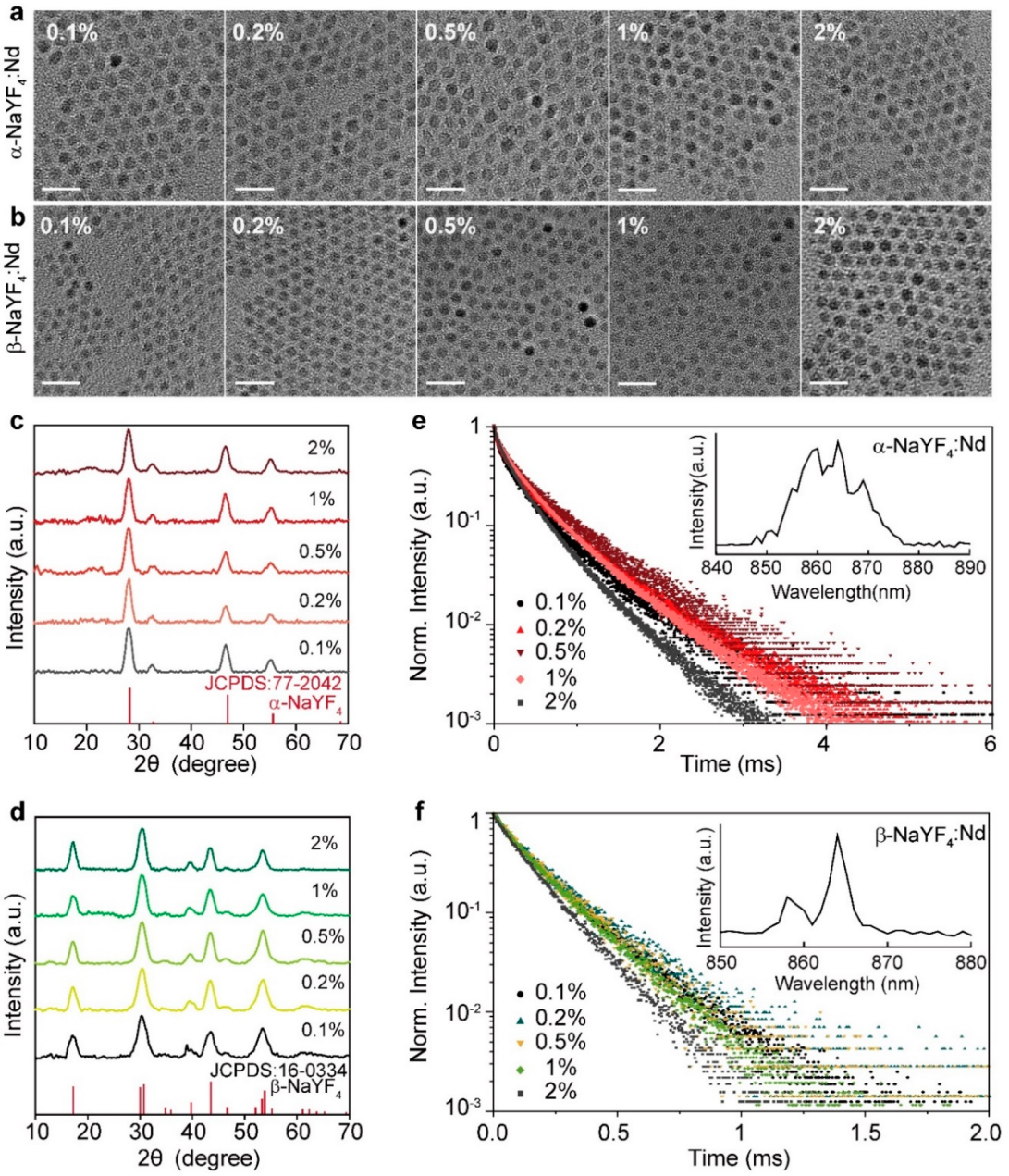

Figure 2. Characterization of Nd^{3+}-doped $NaYF_4$ nanoparticles. (a, b) TEM images of α-$NaYF_4$:x%Nd and β-$NaYF_4$:x%Nd nanoparticles (x = 0.1, 0.2, 0.5, 1, and 2). The scale bar is 20 nm. (c, d) XRD patterns of α-$NaYF_4$:x%Nd and β-$NaYF_4$:x%Nd nanoparticles (x = 0.1, 0.2, 0.5, 1, and 2). (e, f) Luminescence lifetime measurements of α-$NaYF_4$:x%Nd and β-$NaYF_4$:x%Nd nanoparticles (x = 0.1, 0.2, 0.5, 1, and 2). The insets show the corresponding emission spectra under 808 nm excitation.

lifetime of Nd^{3+} due to the short-range cross-relaxation between Nd^{3+}, which is less susceptible to surface quenching.[38]

In response to 808 nm excitation, both α- and β-$NaYF_4$:Nd nanocrystals showed a characteristic luminescence band concentrated around 864 nm due to the optical transition of $^4F_{3/2} \rightarrow {}^4I_{9/2}$ of Nd^{3+} (Figure 2e,f). The decay profiles of α-$NaYF_4$:Nd nanoparticles show that the longest luminescence lifetime was achieved at a doping concentration of 0.5% (Figure 2e and Table S2). Further increase in doping concentration leads to a gradual decrease in luminescence lifetime, which can be ascribed to cross-relaxation-mediated concentration quenching. By comparison, the concentration quenching threshold measured in β-$NaYF_4$:Nd nanoparticles is 0.2%, which is 2.5-fold lower than its cubic counterpart (Table S2). This suggests that hexagonal phase nanoparticles have a shorter average distance between Nd^{3+} ions than cubic nanoparticles, although cubic nanoparticles have a higher doping concentration.

To investigate the influence of surface quenchers on the quenching threshold, we coated cubic and hexagonal $NaYF_4$ nanoparticles with an inert thin shell. The average diameter of α-$NaYF_4$:Nd@$NaYF_4$ nanoparticles obtained at different doping concentrations ranges from 7.0 to 7.8 nm with a shell thickness of ∼0.5 nm (Figure S5). At all doping concentrations, β-$NaYF_4$:Nd@$NaYF_4$ nanoparticles have an average diameter of 6.7 nm and a shell thickness of ∼0.85 nm (Figure S5). The corresponding XRD patterns can be indexed to the standard card data of cubic and hexagonal $NaYF_4$

https://doi.org/10.1021/acs.nanolett.2c04454
Nano Lett. 2023, 23, 979−984

crystals, indicative of pure phases of the nanocrystals (Figure 3a,c). As with core nanoparticles, the luminescence spectra of these core−shell nanoparticles also show an emission band centered at 864 nm (Figure S6).

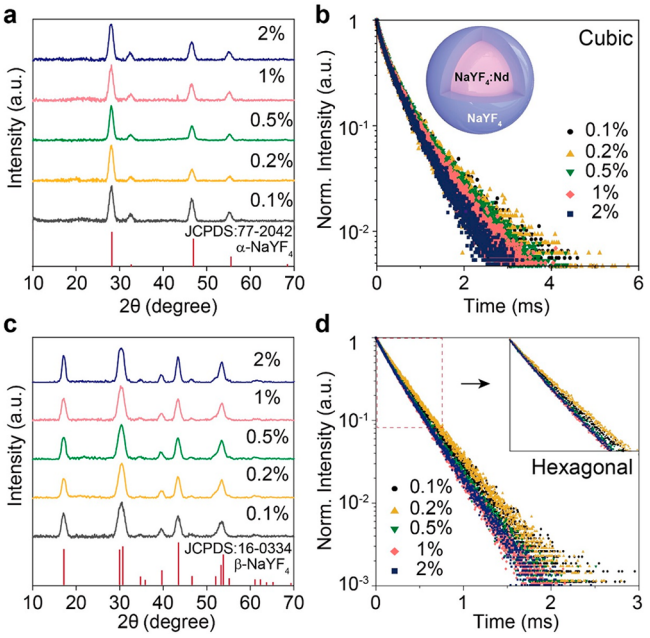

Figure 3. Characterization of Nd^{3+}-doped $NaYF_4$ core−shell nanoparticles. (a, b) XRD patterns and luminescence lifetime measurements of α-$NaYF_4$:*x*%Nd@$NaYF_4$ nanoparticles (x = 0.1, 0.2, 0.5, 1, and 2). (c, d) XRD patterns and luminescence lifetime measurements of β-$NaYF_4$:*x*%Nd@$NaYF_4$ nanoparticles (x = 0.1, 0.2, 0.5, 1, and 2).

For cubic core−shell nanoparticles, we found slight differences in luminescence lifetime between samples doped with 0.1%, 0.2%, and 0.5% Nd^{3+}. Notably, further increase in Nd^{3+} doping favored cross-relaxation-mediated nonradiative decay and shortened the luminescence lifetime (Figure 3b and Table S3). For hexagonal core−shell nanoparticles, the longest luminescence lifetime was achieved in the samples containing 0.2% Nd^{3+} (Table S3). Taken together, the quenching thresholds for cubic and hexagonal core−shell nanoparticles are 0.5% and 0.2%, respectively, which are at the same level as for the core nanoparticles (Figure 3d). This suggests that shell passivation has a negligible influence on multipolar interactions between Nd^{3+} ions.

DFT calculations reveal that the preferential substitution in the β-$NaYF_4$ lattice is closely related to the release of dopant-induced lattice strain at two Y sites. In this regard, a transition from preferential substitution to random replacement should be achieved by modulating the lattice strain via alkaline metal codoping (Figure 4a). We chose Li^+ and K^+ as model ions because they have the same valence as Na^+, and their ionic sizes follow the sequence $R_{Li} < R_{Na} < R_K$. Because isovalent substitution does not generate lattice defects, the replacement of Na^+ by Li^+/K^+ should be able to tailor the lattice strain at Y_1 and Y_2 sites through volume contraction or expansion. Indeed, upon potassium doping, the release of Nd-associated lattice strain at Y_1 and Y_2 decreases the energy of the systems by 0.14 and 0.16 eV, respectively. These comparable strain energies suggest that Nd replaces Y_1 and Y_2 with equal probability. Additionally, the difference in bond length between Y_1−F and

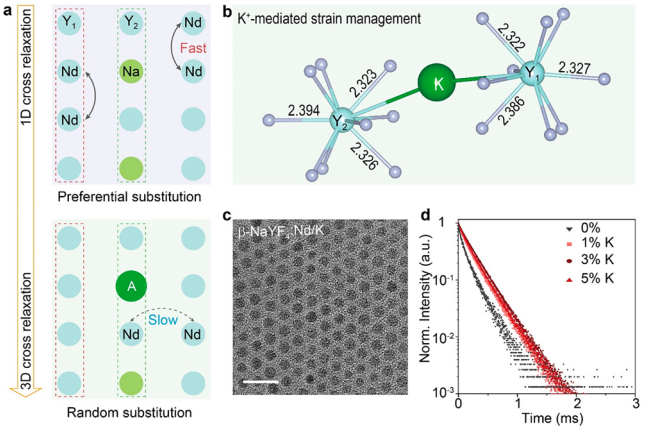

Figure 4. Characterization of β-$NaYF_4$:0.2%Nd nanoparticles codoped with K^+. (a) Schematic of alkali metal-induced transition from preferential to random substitution. A represents Li^+/K^+. (b) DFT-optimized atomic structure of K^+-doped β-$NaYF_4$ lattice. Gray spheres denote fluoride atoms. (c) TEM image of β-$NaYF_4$:0.2% Nd,1%K nanoparticles. The scale bar is 20 nm. (d) Luminescence lifetime of β-$NaYF_4$:0.2%Nd nanoparticles codoped with K^+ at different concentrations (1%, 3%, and 5%).

Y_2−F decreases, suggesting a greater similarity between the coordination configurations of Y_1 and Y_2 sites (Figure 4b). A similar trend was observed in the change of strain energy in β-$NaYF_4$ lattices codoped with Li^+ and Nd^{3+} (Figures S7 and S8).

We next synthesized a series of β-$NaYF_4$ nanoparticles codoped with Nd^{3+} and K^+ or Li^+ at different doping concentrations. The Nd^{3+} concentration was fixed at 0.2%, which is the optimal concentration obtained in Nd^{3+}-doped hexagonal phase nanoparticles. An average diameter of ∼5.8 nm was measured for β-$NaYF_4$:0.2%Nd,*x*%K (x = 1, 3, and 5) nanoparticles (Figures 4c and S9). The presence of K^+ in the as-prepared samples was confirmed by inductively coupled plasma (ICP) analysis. The phase, morphology, and 864-nm emission band of the nanoparticles change negligibly upon potassium doping, irrespective of the K^+ concentration. These β-$NaYF_4$:Nd/K nanoparticles show prolonged luminescence lifetimes, with the longest lifetime of 246 μs obtained at 3% K^+ (Figure 4d and Table S4). For β-$NaYF_4$:0.2%Nd,*x*%Li (x = 1, 3, and 5) nanoparticles, an average diameter of ∼6 nm was determined (Figure S10). XRD characterization confirms the pure hexagonal phase of these codoped samples. Additionally, the center of the emission band remains unaltered upon Li^+ doping. As with K^+-doped nanoparticles, we observed a marked increase in the luminescence lifetime of Nd^{3+} with increasing Li^+ concentration (Figure S11). Specifically, the longest lifetime was obtained for the nanoparticles with 3% Li^+ (Table S4). Lithium or potassium doping extends the lifetime of $^4F_{3/2}$ emission at 864 nm, indicating less cross-relaxation-induced deactivation.

Due to their small ionic size, Li^+ ions are likely to diffuse from oxide and fluoride nanocrystals during washing and centrifugation.[39] Li^+ ions were not detected by ICP in samples prepared with different Li^+ concentrations. Considering that the nanocrystals under study have a high surface-to-volume ratio, it is likely that lithium diffuses to nanocrystal surfaces, especially under high temperatures. Therefore, we speculate that Li^+ ions occupy the sites of Na^+ ions during crystal nucleation and growth. Once occupied, these Li^+ ions could

https://doi.org/10.1021/acs.nanolett.2c04454
Nano Lett. 2023, 23, 979−984

minimize coordination differences between Y_1 and Y_2 sites, alleviate the preferential substitution of Nd^{3+} for Y^{3+} ions, and diffuse toward nanocrystal surfaces with the aid of thermal fluctuation and centrifugal forces.

In conclusion, our work has demonstrated that light lanthanides (La−Sm) preferentially substitute for host Y^{3+} ions in β-$NaYF_4$ nanocrystals at low doping levels. Light lanthanide dopants tend to form Ln−Ln dimers or chain-like clusters, resulting in short interatomic distances and fast energy transfer. We observed a 2.5-fold lower concentration quenching threshold in hexagonal $NaYF_4$:Nd nanocrystals than in their cubic counterparts. It is also possible to manipulate the lattice strain via alkaline metal doping to alter the preferential substitution. This study demonstrates how isovalent doping in inorganic crystal lattices can be utilized to control dopant distribution, opening up a wide range of tailor-made designs of materials and properties.

■ ASSOCIATED CONTENT

Supporting Information

The Supporting Information is available free of charge at https://pubs.acs.org/doi/10.1021/acs.nanolett.2c04454.

Materials; details of synthetic methods, computational models and calculation procedures; physical characterization of lanthanide-doped nanocrystals, including XRD and TEM studies; photoluminescence spectroscopy; DFT-optimized atomic structures and the corresponding electronic energies (PDF)

■ AUTHOR INFORMATION

Corresponding Authors

Xiaogang Liu − *SZU-NUS Collaborative Innovation Center for Optoelectronic Science & Technology, International Collaborative Laboratory of 2D Materials for Optoelectronics Science and Technology of Ministry of Education, Institute of Microscale Optoelectronics, Shenzhen University, Shenzhen, China 518060; Department of Chemistry, National University of Singapore, Singapore 117543;* orcid.org/0000-0003-2517-5790; Email: chmlx@nus.edu.sg

Xian Qin − *Department of Chemistry, National University of Singapore, Singapore 117543*; Email: chmqinx@nus.edu.sg

Authors

Hongyu Bian − *SZU-NUS Collaborative Innovation Center for Optoelectronic Science & Technology, International Collaborative Laboratory of 2D Materials for Optoelectronics Science and Technology of Ministry of Education, Institute of Microscale Optoelectronics, Shenzhen University, Shenzhen, China 518060; Department of Chemistry, National University of Singapore, Singapore 117543*

Caisheng Tang − *Department of Chemistry, National University of Singapore, Singapore 117543*

He Zhao − *Department of Chemistry, National University of Singapore, Singapore 117543*

Complete contact information is available at: https://pubs.acs.org/10.1021/acs.nanolett.2c04454

Notes

The authors declare no competing financial interest.

■ ACKNOWLEDGMENTS

This work was supported by the Agency for Science, Technology and Research (A*STAR) RIE2025 MTC Programmatic Fund (Grant M21J9b0085), National Research Foundation, Singapore, and A*STAR under its Quantum Engineering Programme (NRF2021-QEP2-03-P10), and National Research Foundation, the Prime Minister's Office of Singapore, under its NRF Investigatorship Programme (Award NRF-NRFI05-2019-0003).

■ REFERENCES

(1) Dong, H.; Sun, L.-D.; Yan, C.-H. Energy transfer in lanthanide upconversion studies for extended optical applications. *Chem. Soc. Rev.* **2015**, *44*, 1608−1634.

(2) Haase, M.; Schäfer, H. Upconverting nanoparticles. *Angew. Chem., Int. Ed.* **2011**, *50*, 5808−5829.

(3) Jaque, D.; Vetrone, F. Luminescence nanothermometry. *Nanoscale* **2012**, *4*, 4301−4326.

(4) Li, Y.; Gecevicius, M.; Qiu, J. Long persistent phosphors-from fundamentals to applications. *Chem. Soc. Rev.* **2016**, *45*, 2090−136.

(5) Zheng, B.; Fan, J.; Chen, B.; Qin, X.; Wang, J.; Wang, F.; Deng, R.; Liu, X. Rare-earth doping in nanostructured inorganic materials. *Chem. Rev.* **2022**, *122*, 5519−5603.

(6) Zhou, J.; Liu, Q.; Feng, W.; Sun, Y.; Li, F. Upconversion luminescent materials: advances and applications. *Chem. Rev.* **2015**, *115*, 395−465.

(7) Hemmer, E.; Acosta-Mora, P.; Mendez-Ramos, J.; Fischer, S. Optical nanoprobes for biomedical applications: shining a light on upconverting and near-infrared emitting nanoparticles for imaging, thermal sensing, and photodynamic therapy. *J. Mater. Chem. B* **2017**, *5*, 4365−4392.

(8) Huang, K.; Dou, X.; Zhang, Y.; Gao, X.; Lin, J.; Qu, J.; Li, Y.; Huang, P.; Han, G. Enhancing light and X-ray charging in persistent luminescence nanocrystals for orthogonal afterglow anti-counterfeiting. *Adv. Funct. Mater.* **2021**, *31*, 2009920.

(9) Lay, A.; Siefe, C.; Fischer, S.; Mehlenbacher, R. D.; Ke, F.; Mao, W. L.; Alivisatos, A. P.; Goodman, M. B.; Dionne, J. A. Bright, Mechanosensitive upconversion with cubic-phase heteroepitaxial core-shell nanoparticles. *Nano Lett.* **2018**, *18*, 4454−4459.

(10) Ou, X.; Qin, X.; Huang, B.; Zan, J.; Wu, Q.; Hong, Z.; Xie, L.; Bian, H.; Yi, Z.; Chen, X.; Wu, Y.; Song, X.; Li, J.; Chen, Q.; Yang, H.; Liu, X. High-resolution X-ray luminescence extension imaging. *Nature* **2021**, *590*, 410−415.

(11) Pei, P.; Chen, Y.; Sun, C.; Fan, Y.; Yang, Y.; Liu, X.; Lu, L.; Zhao, M.; Zhang, H.; Zhao, D.; Liu, X.; Zhang, F. X-ray-activated persistent luminescence nanomaterials for NIR-II imaging. *Nat. Nanotechnol.* **2021**, *16*, 1011−1018.

(12) Tsang, M.-K.; Bai, G.; Hao, J. Stimuli responsive upconversion luminescence nanomaterials and films for various applications. *Chem. Soc. Rev.* **2015**, *44*, 1585−1607.

(13) Wen, S.; Zhou, J.; Schuck, P. J.; Suh, Y. D.; Schmidt, T. W.; Jin, D. Future and challenges for hybrid upconversion nanosystems. *Nat. Photonics* **2019**, *13*, 828−838.

(14) Wisser, M. D.; Fischer, S.; Siefe, C.; Alivisatos, A. P.; Salleo, A.; Dionne, J. A. Improving quantum yield of upconverting nanoparticles in aqueous media via emission sensitization. *Nano Lett.* **2018**, *18*, 2689−2695.

(15) Yang, Y. M.; Li, Z. Y.; Zhang, J. Y.; Lu, Y.; Guo, S. Q.; Zhao, Q.; Wang, X.; Yong, Z. J.; Li, H.; Ma, J. P.; Kuroiwa, Y.; Moriyoshi, C.; Hu, L. L.; Zhang, L. Y.; Zheng, L. R.; Sun, H. T. X-ray-activated long persistent phosphors featuring strong UVC afterglow emissions. *Light. Sci. Appl.* **2018**, *7*, 88.

(16) Zhuang, Y.; Chen, D.; Chen, W.; Zhang, W.; Su, X.; Deng, R.; An, Z.; Chen, H.; Xie, R.-J. X-ray-charged bright persistent luminescence in $NaYF_4$:Ln^{3+}@$NaYF_4$ nanoparticles for multidimensional optical information storage. *Light Sci. Appl.* **2021**, *10*, 132.

(17) Dong, H.; Sun, L. D.; Yan, C. H. Local structure engineering in lanthanide-doped nanocrystals for tunable upconversion emissions. *J. Am. Chem. Soc.* **2021**, *143*, 20546−20561.
(18) Fischer, S.; Bronstein, N. D.; Swabeck, J. K.; Chan, E. M.; Alivisatos, A. P. Precise tuning of surface quenching for luminescence enhancement in core-shell lanthanide-doped nanocrystals. *Nano Lett.* **2016**, *16*, 7241−7247.
(19) Liu, S.; Yan, L.; Huang, J.; Zhang, Q.; Zhou, B. Controlling upconversion in emerging multilayer core-shell nanostructures: from fundamentals to frontier applications. *Chem. Soc. Rev.* **2022**, *51*, 1729−1765.
(20) Xu, J.; Dong, Z.; Asbahi, M.; Wu, Y.; Wang, H.; Liang, L.; Ng, R. J. H.; Liu, H.; Vallée, R. A. L.; Yang, J. K. W.; Liu, X. Multiphoton upconversion enhanced by deep subwavelength near-field confinement. *Nano Lett.* **2021**, *21*, 3044−3051.
(21) Zuo, J.; Sun, D.; Tu, L.; Wu, Y.; Cao, Y.; Xue, B.; Zhang, Y.; Chang, Y.; Liu, X.; Kong, X.; Buma, W. J.; Meijer, E. J.; Zhang, H. Precisely tailoring upconversion dynamics via energy migration in core-shell nanostructures. *Angew. Chem., Int. Ed.* **2018**, *130*, 3108−3112.
(22) Chen, B.; Wang, F. Recent advances in the synthesis and application of Yb-based fluoride upconversion nanoparticles. *Inorg. Chem. Front.* **2020**, *7*, 1067−1081.
(23) Cheng, X.; Tu, D.; Zheng, W.; Chen, X. Energy transfer designing in lanthanide-doped upconversion nanoparticles. *Chem. Commun.* **2020**, *56*, 15118−15132.
(24) Feng, M.; Lv, R.; Xiao, L.; Hu, B.; Zhu, S.; He, F.; Yang, P.; Tian, J. Highly erbium-doped nanoplatform with enhanced red emission for dual-modal optical-imaging-guided photodynamic Therapy. *Inorg. Chem.* **2018**, *57*, 14594−14602.
(25) Johnson, N. J. J.; He, S.; Diao, S.; Chan, E. M.; Dai, H.; Almutairi, A. Direct evidence for coupled surface and concentration quenching dynamics in lanthanide-doped nanocrystals. *J. Am. Chem. Soc.* **2017**, *139*, 3275−3282.
(26) Rabouw, F. T.; Prins, P. T.; Villanueva-Delgado, P.; Castelijns, M.; Geitenbeek, R. G.; Meijerink, A. Quenching Pathways in $NaYF_4:Er^{3+}$, Yb^{3+} upconversion nanocrystals. *ACS Nano* **2018**, *12*, 4812−4823.
(27) Wen, S.; Zhou, J.; Zheng, K.; Bednarkiewicz, A.; Liu, X.; Jin, D. Advances in highly doped upconversion nanoparticles. *Nat. Commun.* **2018**, *9*, 2415.
(28) Yang, Y.; Tu, D.; Zhang, Y.; Zhang, P.; Chen, X. Recent advances in design of lanthanide-containing NIR-II luminescent nanoprobes. *iScience* **2021**, *24*, 102062.
(29) Pan, G.; Bai, X.; Yang, D.; Chen, X.; Jing, P.; Qu, S.; Zhang, L.; Zhou, D.; Zhu, J.; Xu, W.; Dong, B.; Song, H. Doping lanthanide into perovskite nanocrystals: highly improved and expanded optical properties. *Nano Lett.* **2017**, *17*, 8005−8011.
(30) Yang, Y.; Lou, B.; Ou, Y.; Su, F.; Ma, C. G.; Duan, C. K.; Dorenbos, P.; Liang, H. Experimental and theoretical studies of the site occupancy and luminescence of Ce^{3+} in $LiSr_4(BO_3)_3$ for potential X-ray detecting applications. *Inorg. Chem.* **2022**, *61*, 7654−7662.
(31) Yao, G.; Berry, M. T.; May, P. S.; Kilin, D. DFT calculation of russell-saunders splitting for lanthanide ions doped in hexagonal (β)-$NaYF_4$ nanocrystals. *J. Phys. Chem. C* **2013**, *117*, 17177−17185.
(32) Xia, Z.; Ma, C.; Molokeev, M. S.; Liu, Q.; Rickert, K.; Poeppelmeier, K. R. Chemical unit cosubstitution and tuning of photoluminescence in the $Ca_2(Al_{1-x}Mg_x)(Al_{1-x}Si_{1+x})O_7:Eu^{2+}$ phosphor. *J. Am. Chem. Soc.* **2015**, *137*, 12494−12497.
(33) Buisson, R.; Vial, J.C. J. *Physique Lett.* **1981**, *42*, 115−118.
(34) Xie, X.; Gao, N.; Deng, R.; Sun, Q.; Xu, Q.-H.; Liu, X. Mechanistic investigation of photon upconversion in Nd^{3+}-sensitized core-shell nanoparticles. *J. Am. Chem. Soc.* **2013**, *135*, 12608−12611.
(35) Cheng, X.; Zhou, J.; Yue, J.; Wei, Y.; Gao, C.; Xie, X.; Huang, L. Recent development in sensitizers for lanthanide-doped upconversion luminescence. *Chem. Rev.* **2022**, *122*, 15998−16050.
(36) Ortgies, D. H.; Tan, M.; Ximendes, E. C.; del Rosal, B.; Hu, J.; Xu, L.; Wang, X.; Martín Rodríguez, E.; Jacinto, C.; Fernandez, N.; Chen, G.; Jaque, D. Lifetime-encoded infrared-emitting nanoparticles for in vivo multiplexed imaging. *ACS Nano* **2018**, *12*, 4362−4368.
(37) Ding, M.-Y.; Lu, C.-H.; Huang, W.-J.; Jiang, C.-F.; Ni, Y.-R.; Xu, Z.-Z. Effect of heat-treatment temperature on upconversion luminescence of β-$NaYF_4:Yb^{3+}$, Er^{3+} nano/microparticles. *J. Inorg. Mater.* **2013**, *28*, 146−152.
(38) Fan, J.; Liang, L.; Gu, Y.; Liu, X. Opposing effects of energy migration and cross-relaxation on surface sensitivity of lanthanide-doped nanocrystals. *Opt. Mater. X* **2021**, *12*, 100104.
(39) Debasu, M. L.; Riedl, J. C.; Rocha, J.; Carlos, L. D. The role of Li^+ in the upconversion emission enhancement of $(YYbEr)_2O_3$ nanoparticles. *Nanoscale* **2018**, *10*, 15799−15808.

https://doi.org/10.1021/acs.nanolett.2c04454
Nano Lett. 2023, 23, 979−984